Supporting Information

For

Electrocatalysis of NO to NH_3 on Transition-metal Doped Two-dimensional BC_2N: A DFT Study

Submitted to ***Physical Chemistry Chemical Physics***

by

Zehua Long[a,b], Chenrong Wang[a], Wei Zhang[a], Shansong Sheng[a], Jiajia Wang[b,*], Donghui Yang[b,c,*]

a. CHN Energy Tongling Power Generation Co., Ltd., Tongling 244100, China

b. College of Materials Science and Engineering, Hohai University, Changzhou 213200, China

c. Suqian Research Institute of Hohai University, Suqian 223814, China

* Corresponding authors: xcrysden@163.com (J. Wang), donghuiyang@hhu.educn (D. Yang)

Table S1 compares the binding energies of single metal atoms on BC_2N substrates with either B or N vacancies. It is evident that metal atoms exhibit lower binding energies at B vacancy sites, and all values are negative, indicating higher thermodynamics stability and the spontaneous nature of the doping process. The detailed binding energy values are as follows.

Table S1. E_b of single transition-metal atoms doped at single B and N vacancy sites on two-dimensional BC_2N substrates.

$B_V@BC_2N$	E_b（eV）	$N_V@BC_2N$	E_b（eV）
Ti	-3.87	Ti	1.81
V	-2.50	V	2.57
Cr	-1.99	Cr	2.67
Mn	-2.26	Mn	1.90
Fe	-3.05	Fe	0.46
Co	-2.90	Co	-0.31
Ni	-1.89	Ni	0.02
Zr	-3.59	Zr	2.00
Nb	-1.69	Nb	2.81
Mo	-0.77	Mo	3.23
Ru	-1.54	Ru	1.05
Rh	-2.03	Rh	-0.61
Pd	-0.87	Pd	-0.08

Table S2 presents the free energy comparison between the initial NO adsorption step of the NORR-to-NH_3 pathway and the competing HER process on $TM@BC_2N$. The results indicate that upon TM doping, the free energies of HER are significantly higher than those of NO adsorption, suggesting that hydrogen evolution is suppressed and NO adsorption is energetically favored.

Table S2. Gibbs free energies of three different NO adsorption configurations and the HER on $TM@BC_2N$ substrates. F denotes that the corresponding adsorption configuration is not stable.

$TM@BC_2N$	N-end(eV)	NO-side(eV)	O-end(eV)	HER(eV)
Ti	-2.10	-2.13	-1.29	-0.83
V	-2.96	-2.99	-1.72	-0.83
Cr	-3.39	-3.23	-1.60	-0.73
Mn	-2.93	-2.12	-1.42	-0.59
Fe	-2.45	F	-1.13	-0.36
Co	-1.71	F	-0.39	0.36
Ni	-2.05	F	-0.66	0.05
Zr	-1.96	-2.07	-1.16	-1.16
Nb	-2.996	-3.33	-1.73	-1.73
Mo	-3.51	-3.87	-2.10	-2.10
Ru	-2.58	F	-1.23	-0.51
Rh	-1.48	F	-0.20	0.25
Pd	-1.81	F	-0.53	-0.25

In the hydrogenation pathway analysis, distinct variations in the RDS were observed among different $TM@BC_2N$ systems. For $Ti@BC_2N$, $V@BC_2N$, $Cr@BC_2N$, $Zr@BC_2N$, $Nb@BC_2N$, $Mo@BC_2N$, and $Pd@BC_2N$, the $NH_2 \rightarrow NH_3$ conversion constitutes the primary RDS, whereas for $Mn@BC_2N$, $Fe@BC_2N$, $Ni@BC_2N$, and $Ru@BC_2N$, the RDS occurs at the NO → NHO step. These findings indicate that both the initial and terminal hydrogenation stages play particularly critical roles in determining the overall kinetics of NORR (see **Figure S1**).

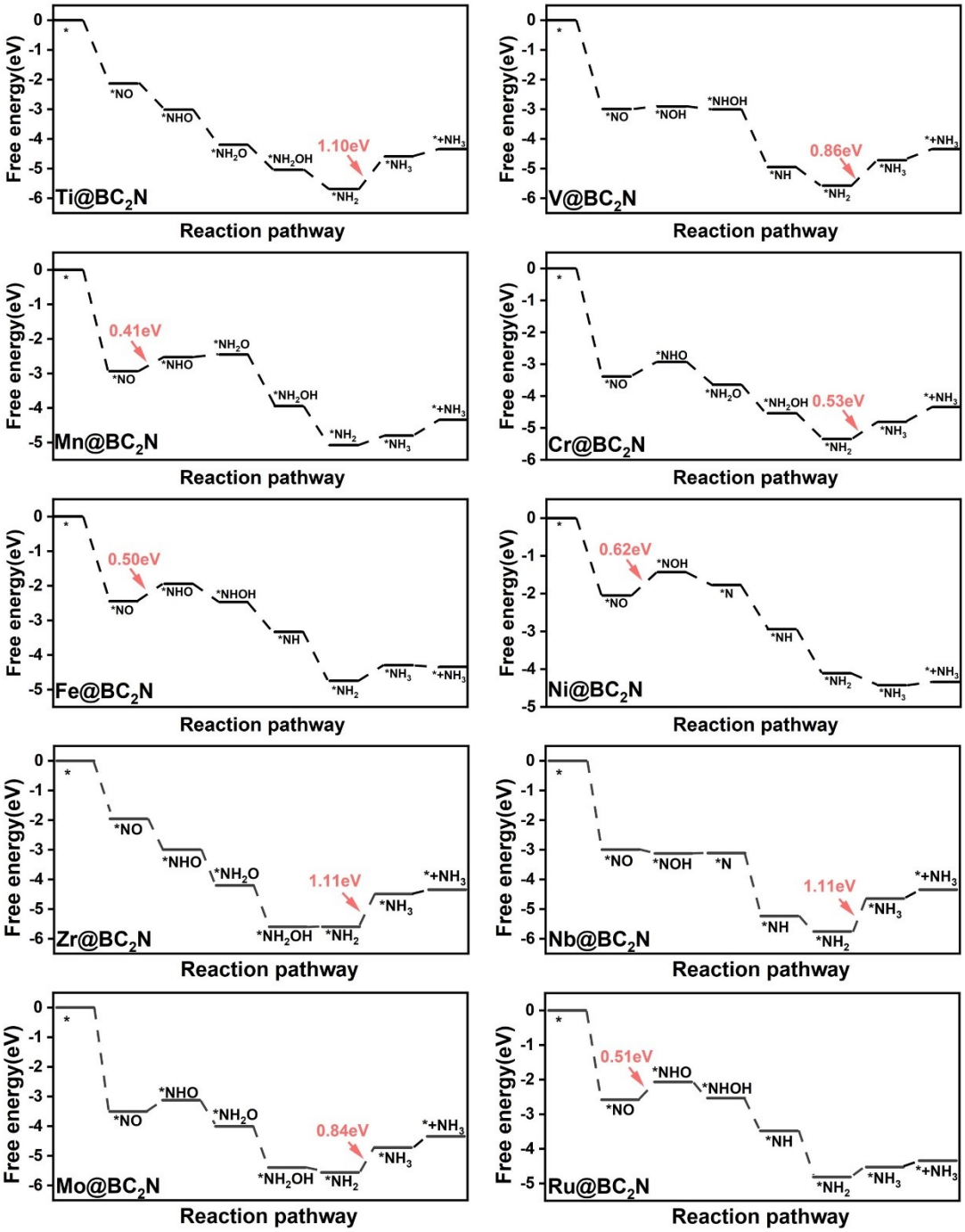

Figure S1. Gibbs free energy diagrams for NORR-to-NH_3 pathways on the remaining TM@BC_2N substrates.

The full Gibbs free-energy diagrams (see **Figure S2**) enable a more comprehensive comparison among the possible hydrogenation sequences and further substantiate the identification of the most favorable pathway for each catalyst.

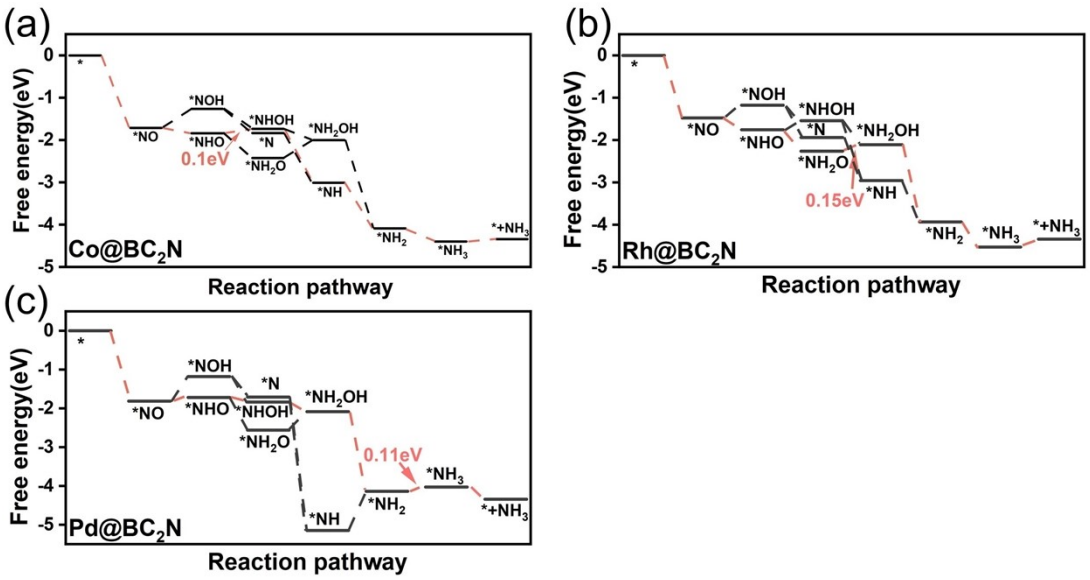

Figure S2. Optimal NORR pathways on Co@BC_2N, Rh@BC_2N, and Pd@BC_2N(a-c). Complete free-energy diagrams including all intermediates.

The results of **Table S3** show that the NH_3 desorption energies remain moderate for the highly active candidates, including Co@BC_2N, Rh@BC_2N, and Pd@BC_2N, and stay within a feasible range (< 0.2 eV). Moreover, as reported previously, NH_3 can be further protonated to NH_4^+ under acidic conditions, which facilitates product release from the catalyst surface (ACS Catalysis, 2017, 7, 6, 3869-3882). Therefore, although NH_3 desorption requires an additional energetic step, it does not alter the overall conclusion that Co@BC_2N remains the most promising candidate for NORR.

Table S3. Calculated NH_3 desorption free energies on TM@BC_2N.

TM@BC_2N	Desorption Free Energy (eV)	TM@BC_2N	Desorption Free Energy (eV)
Ti	0.25	Zr	0.14
V	0.38	Nb	0.30
Cr	0.47	Mo	0.38
Mn	0.46	Ru	0.19
Fe	-0.04	Rh	0.18
Co	0.06	Pd	-0.31
Ni	0.09		

We carried out comparative NORR calculations using the PBEsol functional (see **Figure S3.a, c, e)** Although minor quantitative differences are observed, the key proton-coupled electron transfer (PCET) steps and the corresponding RDS are consistent with those obtained using the PBE functional, with deviations also within 0.1 eV. These cross-checks demonstrate that the main conclusions of this work are reliable and insensitive to the choice of solvation treatment or exchange-correlation functional.

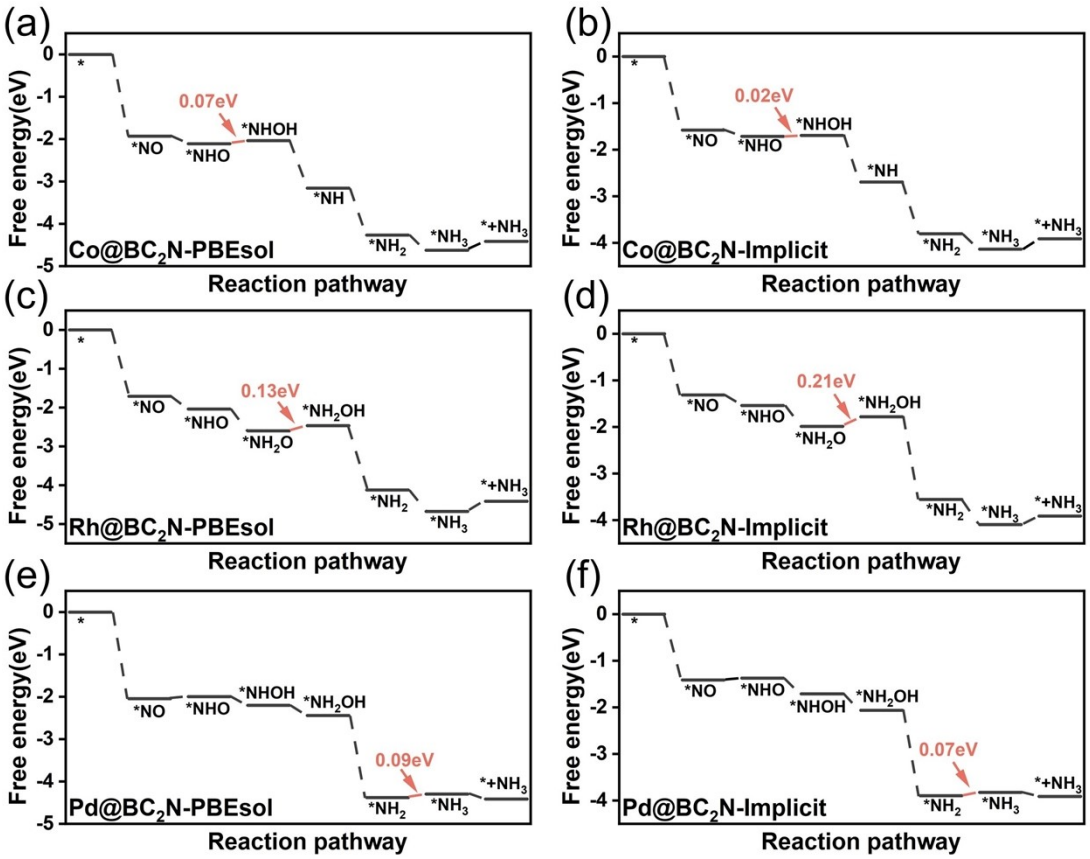

Figure S3. NORR Gibbs free-energy profiles on Co@BC_2N, Rh@BC_2N, and Pd@BC_2N calculated with PBEsol functionals and implicit solvation conditions. (a,c,e) PBEsol results; (b,d,f) VASPsol results.

To address the concern regarding the vacuum slab approximation, we performed additional calculations using an implicit solvation model (VASPsol) for representative systems, namely Co@BC_2N, Rh@BC_2N, and Pd@BC_2N(see **Figure S3 b, d, f)**. The results indicate that the solvation treatment stabilizes the adsorbed intermediates and slightly lowers the rate-determining step (RDS) barriers, while the overall reaction trends and catalyst ranking remain unchanged. Notably, the differences in the key free-energy values are within 0.1 eV, confirming the robustness of our conclusions.

Considering that the variation in RDS is within 0.1 eV, we did not extend the solvation treatment to the remaining ten systems to ensure computational efficiency.